High-Throughput Visual Detection of Multiple Sweat Biomarkers Based on Au@Pt modified Bimetallic MOF-derived Nanozyme Hydrogels

Lijun Ding[a], Xilong Zhou[b], Shilin Wang[b], Hanyang Jiao[b], Dandan Huang[b], Tianshuo Wang[b], Lianxi Pu[b], Jin Shen[b], Min Zhang[b], Deping Wang[b], and Kun Wang[b]*

[a]*School of Agricultural Engineering, Jiangsu University, Zhenjiang 212013, PR China.*

[b]*School of Chemistry and Chemical Engineering, Jiangsu University, Zhenjiang 212013, PR China.*

Content

S1. Experimental section

S1.1 Materials

S1.2 Apparatus

S1.3 The synthesis of CuFe-MOF-400, Au@Pt and Au@Pt/CuFe-MOF-400

S1.4 POD performance test of Au@Pt/CuFe-MOF-400

S2 Results and discussion

S2.1 Optimization of conditions

Figure S1

Figure S2

Figure S3

Figure S4

Figure S5

Table S1

References

S1. Experimental section

S1.1 Materials

Chloroauric acid trihydrate ($HAuCl_4 \cdot 3H_2O$, AR), Copper (II) chloride dihydrate ($CuCl_2 \cdot 2H_2O$, AR), Potassium chloroplatinate (K_2PtCl_6, AR), Vitamin C (VC, AR), N,N-dimethylformamide (DMF, AR), hydrogen peroxide (H_2O_2, GR), from Sinopharm Chemical Reagent Co., Ltd. (China). Polyether F127 (PF127, average Mn ~12,000), Sodium alginate (SA, AR), 2-amino-terephthalic acid (NH_2-BDC, 98%), 3,3',5,5' -tetramethylbenzidine (TMB, 98%), Agarose (Bio-electrophoretic grade) from Shanghai Macklin Biochemical Co., Ltd. Ferric chloride hexahydrate ($FeCl_3 \cdot 6H_2O$, 98%) from Sigma-Aldrich (USA). Polydimethylsiloxane (PDMS) film is purchased from Hangzhou Westru Technology Co., LTD.

S1.2 Apparatus

The morphology of the materials was observed by scanning electron microscopy (SEM, JSM-7800F, Japan). X-ray diffraction (XRD) patterns were recorded by a high-intensity Cu Kα (λ = 1.5406) radiation X-ray diffractometer in Bruker, Germany. The absorption intensity was measured with an ultraviolet-visible spectrophotometer (Cary8454, Agilent, USA). X-ray photoelectron spectroscopy (XPS) measurements were made on Thermo Scientific K-Alpha X-ray photoelectron spectrometer using Al K-alpha X-rays as the excitation source. The specific surface area and pore diameter of the material were measured by Surface Area and Porosity Analyzer (BET, TriStar II 3020, USA). The infrared absorption peak was tested on a Fourier Transform infrared spectrometer (FT-IR, Nicolet iS50, USA). Electron spin resonance (EPR) spectra were recorded on the Bruke-E500 electron paramagnetic resonance spectrometer. Contact angle was measured on the contact angle measuring device (SDC-350KS).

S1.3 The synthesis of CuFe-MOF-400, Au@Pt and Au@Pt/CuFe-MOF-400

The CuFe-MOF was placed in the crucible and then in the muffle furnace. It was calcined at 400°C in a nitrogen atmosphere for 3 hours, with a heating rate of 5 °C/min.

The preparation method of Au@Pt was based on previous references[1]. Specifically, mix PF127 (0.06 g) with 3.0 mL of K_2PtCl_6 solution (20 mM) and 3.0 mL of $HAuCl_4 \bullet 3H_2O$ solution (20 mM) in a small beaker and stir evenly with a magnetic force. Then, add 6.0 mL of AA solution (0.1 M) to the beaker and ultrasonicate the mixture for 15 minutes. Finally, the reactants were settled for 24 hours, centrifuged,

and washed with acetone and water to remove the remaining PF127. Dry at 45℃, grind the collected products, and store them at room temperature.

Add 20 mg of Au@Pt and 80 mg of CuFe-MOF-400 to a beaker, add 40 mL of H_2O, mix well, and stir for 4 h, then centrifuge, wash, and dry.

S1.4 POD performance test of Au@Pt/CuFe-MOF-400

10 μL of Au@Pt/CuFe-MOF-400 dispersion (0.5 mg•mL^{-1}), 340 μL of HOAc-NaOAc buffer (pH=3, 0.1 M), 100 μL of TMB ethanol solution (10 mM), and 50 μL of H_2O_2 solution of different concentrations. After shaking evenly, the reaction was carried out at 37℃ for 5 minutes, and then the ultraviolet absorption peak at 652 nm was measured in the ultraviolet-visible spectrometer.

S1.5 Design and Preparation of sodium alginate (SA) hydrogel

The preparation of sodium alginate (SA) hydrogel referred to previous literature and underwent certain improvements[12]. Specifically, SA was dissolved in HOAc-NaOAc buffer solution (pH=3, 0.1 M) at a concentration of 25 mg·mL^{-1}. During this process, 30 mg of Au@Pt/CuFe-MOF-400, 30 μL of TMB dissolved in EtOH (10 mM), and 10 μL of UAO dispersions were added and stirred together until uniform. Transfer a fixed volume of the well-mixed solution to the mold, and immerse the mold in a $CaCl_2$ solution with a concentration of 30 mg·mL^{-1} for 0.5 hours. After the cross-linking is complete, take out the hydrogel and refrigerate it for future use. The fixed volume of solution was dropped on the rubber mold while it was hot, and then the bubbles were removed by vacuuming and cooled at room temperature to form a round hydrogel patch (d = 0.8 cm, thickness 0.5 mm).

S1.6 Construction of POCT device and gray recognition

For the construction of the POCT detection device, a PDMS patch (d = 2 cm, thickness 2 mm) is purchased from Hangzhou Westru Technology Co., LTD. The hydrogel patch we prepared before is placed in the hole in the three circles of the PDMS patch. There is still some distance between the hydrogel and human skin, which can prevent direct contact between the colorimetry reagent and the human body. Next, the viewing area (Vinyl chloride sticker) is attached above the PDMS patch, and finally, a layer of breathable adhesive is covered above the entire device to ensure that the device can be fully attached to the human skin.

In order to achieve portable biosensing, the "color capture" application in the smart device is used to analyze the gray value of the color. It should be noted that all

photography processes are carried out under LED lights, and try to avoid shadows, in order to protect the consistency of environmental lighting conditions. First, the image of the hydrogel patch after changing color is taken and recorded as image A. Upon capturing the faded hydrogel patch image, denoted as image B, the ΔR value was determined by comparing its gray value intensity with that of image A.

S2 Results and discussion

S2.1 The morphologies of Au@Pt and Au@Pt/CuFe-MOF-400

The morphologies of Au@Pt and Au@Pt/CuFe-MOF-400 were investigated by scanning electron microscopy (SEM). As can be seen from Fig. S1A, the prepared Au@Pt is spherical as a whole, and the solid has a little agglomeration. Further, it was scanned by transmission electron microscopy (TEM), and elemental analysis of its single crystal was performed by EDS. The specific data are shown in Fig. S1B. It can be seen from the figure that Au@Pt is a regular sphere, the overall size of the material is about 50 nm, and the uniform distribution of Au and Pt can be observed by EDS elemental analysis. Indicating the preliminary successful synthesis of Au@Pt. Subsequently, Au@Pt/CuFe-MOF-400 was prepared by room-temperature stirring, and its morphology is shown in Fig. S1C. It can be seen that the uneven surface of CuFe-MOF-400 is loaded with many fine nanoparticles, which are very similar to the morphology of Au@Pt. EDS elemental analysis was performed to demonstrate the successful combination of the two, as shown in Fig. S1D-I, which shows the presence of N, O, Fe, Cu, Au, and Pt elements, indicating the successful combination of Au@Pt and CuFe-MOF-400.

S2.2 Optimization of conditions

Optimal POD performance was achieved by optimizing the doping ratio of Au@Pt and CuFe-MOF-400, reaction temperature, and pH. As shown in Fig. S3A, the best POD performance is achieved when the ratio of Au@Pt to CuFe-MOF-400 reaches 1:4, so the secondary doping ratio is selected in the preparation; As shown in Fig. S3B, Au@Pt/CuFe-MOF-400 exhibits good POD performance when the reaction temperature reaches 30-40 °C, so the reaction temperature is selected between 30-40 °C; Finally, the influence of pH on the enzyme performance during the reaction was explored, as shown in Fig. S3C. It can be seen that when pH=4, better POD performance is achieved. Therefore, pH=4 is selected as the optimal reaction environment.

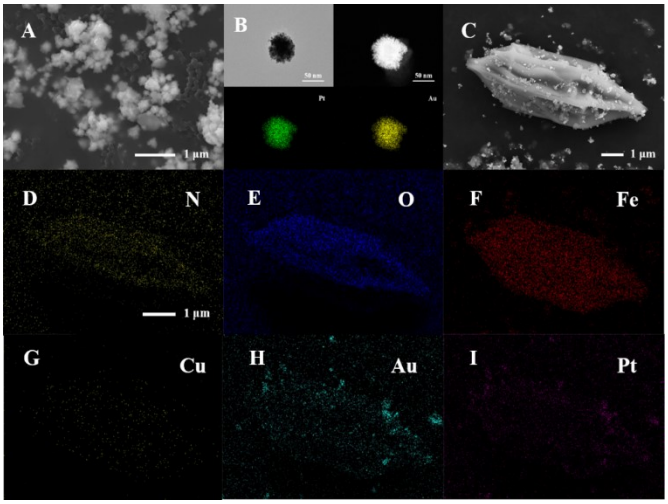

Fig. S1 (A) SEM image of Au@Pt; (B) TEM image of Au@Pt and EDS diagram corresponding to respective elements; (C) SEM image of Au@Pt/CuFe-MOF-400; EDS diagram of N (D), O (E), Fe (F), Cu (G), Au (H), and Pt (I) on Au@Pt/CuFe-MOF-400.

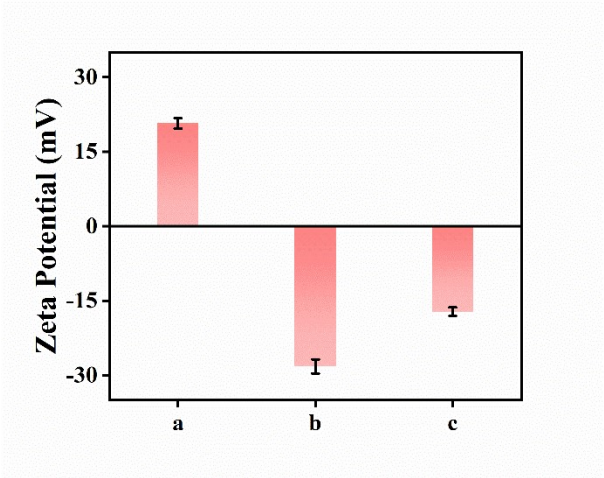

Fig. S2 Zeta potentials of CuFe-MOF-400 (a), Au@Pt (b) and Au@Pt/CuFe-MOF-400 (c). Data are presented as mean±SD (n=3).

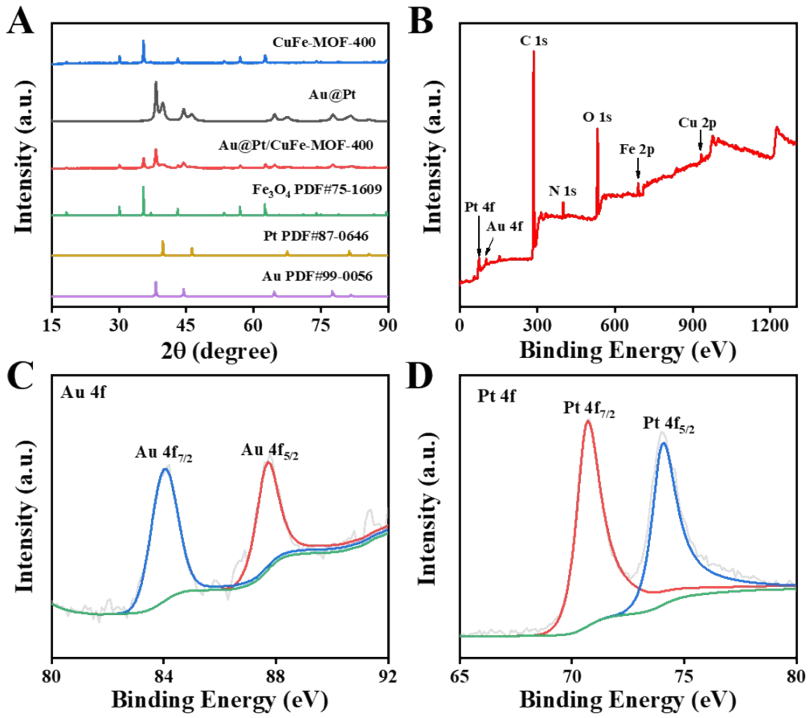

Fig. S3 (A) XRD analysis and comparison of standard spectra of CuFe-MOF-400, Au@Pt and Au@Pt/CuFe-MOF-400; (B) Total XPS scan spectrum of Au@Pt/CuFe-MOF-400; (C) Scan spectra of Au 4f; (D) Scan spectrum of Pt 4f.

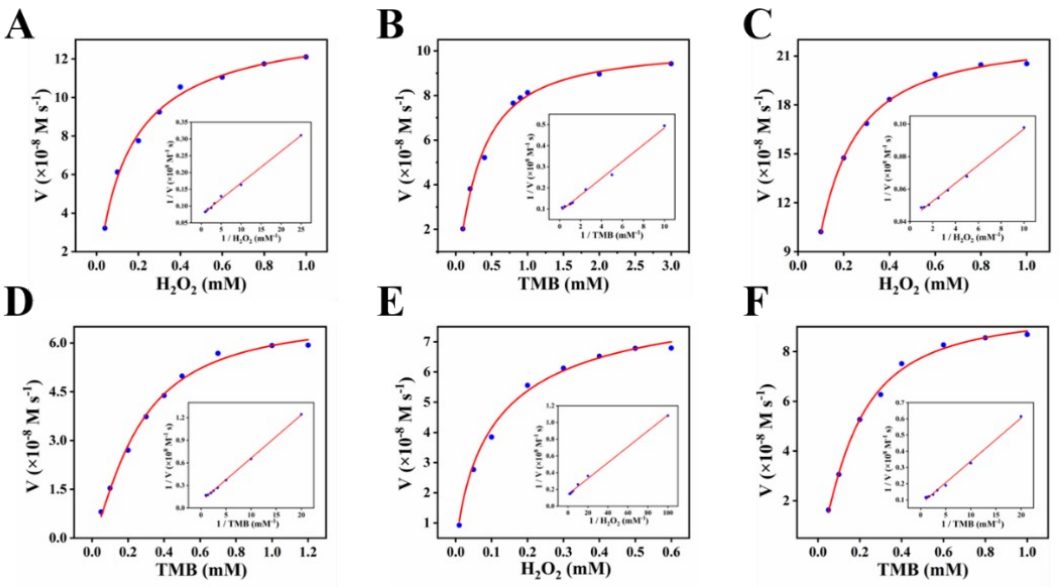

Fig. S4 Steady state kinetic analysis and Lineweaver Burk curve of CuFe-MOF-400 using H_2O_2 (A) and TMB (B) as substrates; steady state kinetic analysis and Lineweaver Burk curve of Au@Pt using H_2O_2 (C) and TMB (D) as substrates; Steady state kinetic analysis and Lineweaver Burk curve of Au@Pt/CuFe-MOF-400 using H_2O_2 (E) and TMB (F) as substrates.

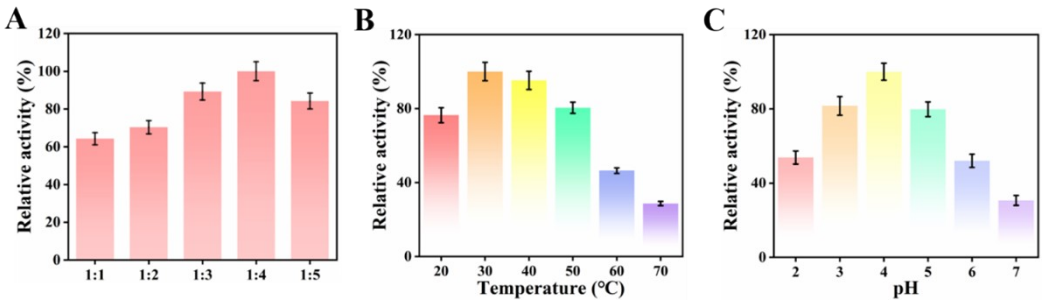

Fig. S5 (A) The effect of the binding ratio of Au@Pt to CuFe-MOF-400 on the POD activities; (B) The relative activity of Au@Pt/CuFe-MOF-400 at different temperatures; (C) The relative activity of Au@Pt/CuFe-MOF-400 at different pH. Data are presented as mean±SD (n=3).

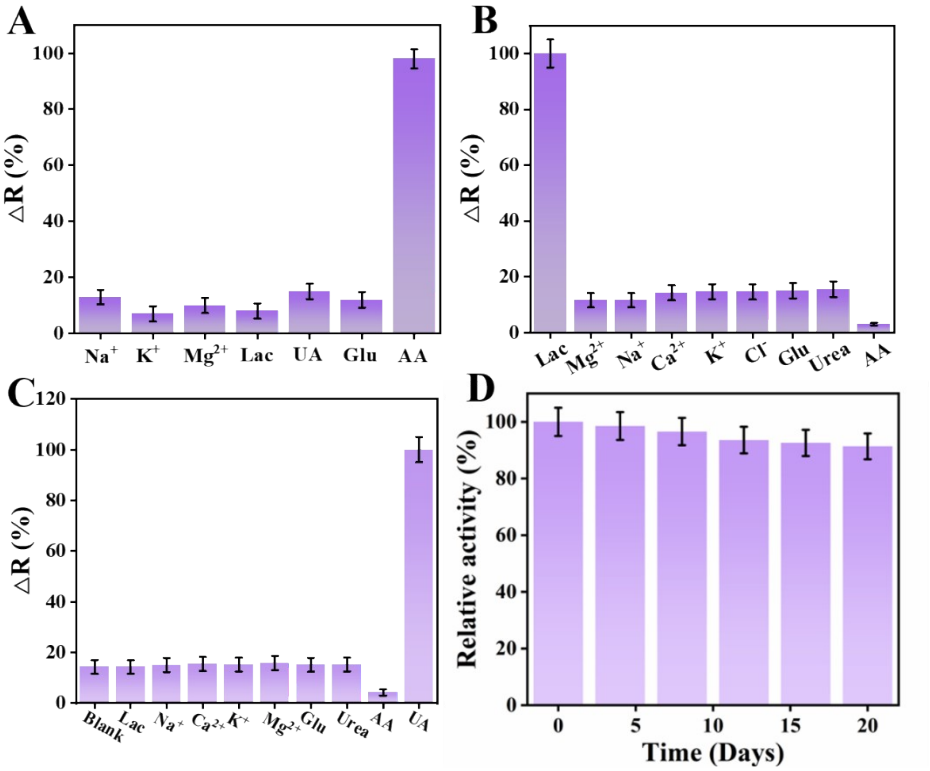

Fig. S6 (A) Selectivity of region A (A), region B (B), regin C (C), and stability of the SA hydrogel patch. Data are presented as mean±SD (n=3).

Table S1 K_m (H_2O_2 and TMB) and Lineweaver-Burk curves

	Catalyst	Lineweaver-Burk	K_m/mM
H_2O_2	CuFe-MOF-400	Y=0.00943 X+0.0744	0.127
	Au@Pt	Y=0.00555 X+0.0504	0.109
	Au@Pt/CuFe-MOF-400	Y=0.00947 X+0.1404	0.067
	HRP	-	3.7
TMB	CuFe-MOF-400	Y=0.03985 X+0.0856	0.458
	Au@Pt	Y=0.05145 X+0.0889	0.578
	Au@Pt/CuFe-MOF-400	Y=0.02656 X+0.0735	0.361
	HRP	-	0.43

1. R. Xu, Y. Yang, M. Xu, Y. Tao, C. Deng, M. Li, D. Wei, Y. Deng, J. Lv, C. Wu and Z. Zhang, *Sensors and Actuators B: Chemical*, 2024, **420**.